Observations of Jets and Outflows from Young Stars

John Bally
University of Colorado at Boulder

Bo Reipurth
University of Hawaii

Christopher J. Davis
Joint Astronomy Centre

This review concentrates on observations of outflows from young stars during the last seven years. Recent developments include detections of an increasing number of Herbig-Haro flows at X-rays and UV wavelengths, high-resolution studies of irradiated jets with HST, wide-field imaging of parsec-scale outflows with groundbased CCDs and near-IR imagers, complete surveys of visual and near-IR emission from shocks in the vicinity of entire molecular clouds with wide-field imagers, far-infrared studies with the Infrared Space Observatory and the Spitzer Space Telescope, and high angular submillimeter, millimeter, and centimeter wavelength aperture synthesis array data cubes showing both the spatial and velocity structure of jets and outflows.

1. INTRODUCTION

Outflows are one of the manifestations of the birth of a young star that are easiest to observe. More than a half century ago, *Herbig* (1950, 1951) and *Haro* (1952, 1953) found the first examples of the peculiar nebulae that have come to be known as Herbig-Haro (HH) objects. Located in or near dark clouds in regions suspected of having undergone recent star formation, HH objects were first thought to be young stars or their associated reflection nebulae. However, by the 1970s, their spectra were interpreted as indicative of mostly low-excitation shock waves. By the 1980s some of the growing list of HH objects were found to trace highly collimated jets powered by young stars (*Dopita et al.,* 1982; *Mundt and Fried,* 1983; *Reipurth et al.,* 1986), associated with high proper-motion bipolar outflows (*Herbig and Jones,* 1981).

During the 1960s and 1970s, additional manifestations of outflow activity were discovered. These include P-Cygni profiles and other spectroscopic indicators of powerful stellar winds emerging from young stars, high-velocity OH and H_2O masers, bipolar molecular outflows (e.g., *Snell et al.,* 1980), as well as shock-excited near-IR emission lines of species such as [FeII] and H_2. By the 1980s, a number of young stellar objects (YSOs) were found to produce radio continuum jets visible at centimeter wavelengths. Although it was not at first apparent, by the early 1990s, observations and theoretical considerations made it clear that most manifestations of outflow activity were produced by shocks powered by forming stars.

The advent of large-format CCDs and the launch of the Hubble Space Telescope (HST) during the 1990s ushered in new developments. Wide-field visual wavelength surveys revealed that outflows can attain parsec-scale dimensions with lengths exceeding 10 pc, and that they blow out of their molecular clouds (*Bally and Devine,* 1994; *Reipurth et al.,* 1997; *Eislöffel and Mundt,* 1997). Narrow-band-filter imaging revealed a new population of protostellar jets in HII regions that are rendered visible by the UV radiation fields of nearby massive stars (*Reipurth et al.,* 1998a; *Cernicharo et al.,* 1998; *Bally and Reipurth,* 2001). HST has resolved the subarcsecond scale structure and cooling layers of dozens of HH objects. HST has enabled the measurement of proper motions on images taken less than one year apart — a timescale shorter than the typical cooling time.

1.1. The Importance of Outflows

Although no theory of star formation anticipated jets and outflows, it is now clear that the production of these flows is a fundamental aspect of star formation. Collimated outflows occur in most astrophysical systems in which accretion, rotation, and magnetic fields interact. Due to their proximity, large numbers [nearly a thousand masers, HH objects, and molecular outflows are now known (*Wu et al.,* 2004)], and diversity of available tracers, protostellar outflows make ideal laboratories for the investigations of the physics, chemistry, acceleration, collimation, propagation, and impacts of these systems. The results of these studies should be relevant to many other classes of astrophysical outflow.

Outflows provide a fossil record of the mass loss and, therefore, mass-accretion histories of forming stars. Outflow symmetries provide clues about the dynamical environment of the engine; S- and Z-shaped symmetries indicate that the outflow axis has changed over time, perhaps due to precession induced by a companion, or interactions with sibling stars in a cluster. C-shaped bends indicate motion of surrounding gas (side winds), or the motion of the outflow

source itself. Outflows have a profound impact on their surroundings. Jets and winds create cavities in the parent cloud and inject energy and momentum into the surrounding gas that, in the absence of massive stars, may dominate the generation of turbulence and cloud motions. The terminal shocks in outflows dissociate molecules, sputter grains, and can reset the chemical evolution of clouds to an initial state. Shocks also drive chemistry, thereby altering the chemical composition of the impacted media. Outflows may play a fundamental role in sculpting and disrupting their parent clouds. They may play a role in determining final stellar masses and the shape of the initial mass function. Outflows may also carry away some of the angular momentum of matter accreting onto the forming star.

This review will concentrate on developments since the last Protostars and Planets conference held in 1998. During the last seven years, observational and computational capabilities have increased greatly. Major new developments include the detection of X-rays from an increasing number of protostellar outflows and the measurement of the emission and absorption spectra of some HH objects in the UV (section 2). At visual and near-IR wavelengths, the formats of detectors have continued to increase with pixel counts doubling approximately every two years. This has led to the first complete imaging surveys of entire giant molecular clouds with 4-m-class telescopes in narrow-band filters sensitive to shock tracers. Eight-meter-class telescopes, adaptive optics, a new generation of high-resolution and multiobject spectrographs, and the Advanced Camera for Surveys on HST have had major impacts (section 3). The Spitzer Space Telescope is surveying the galactic plane and many of the nearby clouds, and IRAC and MIPS images are providing stunning images of the mid-IR emission from jets, outflows, and the properties of their sources. Thermal imaging with Gemini has traced entrained warm dust in jets. Upgrades at the VLA, and a new generation of millimeter-interferometers such as the SMA on Mauna Kea, are producing stunning arcsecond-resolution images of molecular jets, and have enabled the detection of many highly embedded sources invisible at shorter wavelengths (section 4).

1.2. Overview of Outflow Properties and Behavior

The velocity difference between the parent cloud and the outflow correlates with wavelength. Although weak knots of CO emission and jets can sometimes be found at velocities of several hundred km s^{-1} near the core, the bulk of millimeter-wavelength CO emission tends to have velocities of only a few to ten km s^{-1}. While the near-IR lines of H_2 and [FeII] tend to have velocities of several tens of km s^{-1}, the visual wavelength forbidden and recombination lines usually have radial velocities of tens to hundreds of km s^{-1}. X-ray emission is only seen from shocks with speeds higher than 300 km s^{-1}.

This trend can be understood in terms of a unified picture. The YSO accelerates a wind, sometimes collimated into a jet, with a velocity several times the escape speed from the launch region, which can range from 100 to over 500 km s^{-1}. Internal shocks form where faster ejecta overrun slower material. The very fastest shocks can sometimes be detected in X-rays. These primary flows often contain molecules such as H_2, CO, and SiO when launched from young Class 0/I sources; they tend to be dominated by HI and low-ionization metals when the source is more evolved. Jet speeds also tend to increase, and their densities and mass-loss rates tend to decrease with the evolutionary state of the source. In young, high-density molecular jets, these shocks can excite H_2O maser spots and H_2 emission; in mostly atomic or ionized jets from somewhat older sources, knots of Hα and/or forbidden line emission are produced.

The primary jets and winds transfer momentum and entrain their surroundings by means of shock waves propagating into the medium. These shocks tend to have much lower velocities than the jets; they can be seen in H_2 emission when the interaction is with a molecular cloud, or in Hα or forbidden lines when the medium is atomic or ionized. Most molecular emission observed at submillimeter, millimeter, and centimeter wavelengths is produced by gas entrained and accelerated by these secondary shocks.

There are no perfect tracers of outflows; each tracer and every transition provides information about a limited range of physical conditions. A complete picture of outflows therefore requires observations in the radio, submillimeter, IR, visual, UV, and even X-ray portions of the spectrum.

Species such as CO and other molecular transitions probe the mass and radial velocity of swept-up and entrained gas in an outflow, but only in the molecular cloud. When primary jets and winds blow out of their parent clouds, they are no longer visible in molecular transitions. Sometimes, the 21 cm line of HI can be used to trace entrained gas. These species are excited by collisions at the ambient temperature of the cloud and therefore do not require shocks to be observable. CO, other easy-to-excite molecular transitions, and HI trace the total amount of momentum injected into the cloud and the amount of mass accelerated by an outflow over its lifetime. Shocks inside a molecular cloud can sometimes be traced by the near- and mid-IR transitions of H_2 or, if the flow is partially ionized, by species such as [FeII]. At sufficiently low extinctions, or outside the molecular cloud once the outflow has broken out of its natal environment, atomic lines such as Hα and forbidden transitions of atoms and ions such as [OI], [OII], [OIII], [NII], and [SII] in the visual and near-IR can be used to trace shocks and postshock cooling layers. However, these tracers disappear after a cooling time in the postshock gas. The bulk of the moving mass propagating outside a molecular environment can be traced by 21 cm HI if the medium is atomic. In practice, such observations are made very difficult by foreground and background emission from the galaxy. Illumination of the jet or entrained gas by nearby massive stars provides a better opportunity to trace the unshocked portions of outflows propagating outside molecular clouds. In recent years, the study of externally irradiated jets and outflows has shown that such flows are common in HII regions.

Many questions remain unanswered. Are the collimated outflows powered directly by the YSO, its magnetosphere, its circumstellar disk, or by a combination of these sources? Is the X-wind or the disk model more correct? Do both mechanisms coexist? How are winds collimated into jets? How do the properties of outflows change with the evolution of the driving source? How long does jet production persist? Although there are many strongly held opinions, and a few observational constraints, most of these issues remain open. The next generation of interferometers, spectographs, and ultra-high-resolution instruments will be needed to obtain definitive observations.

2. FAST SHOCKS: OBSERVATIONS OF ULTRAVIOLET AND X-RAYS

2.1. X-Ray Results

YSOs have been known to be prolific sources of X-rays and UV radiation (see the chapter by Feigelson et al.). Time-averaged X-ray luminosities range from L_x less than 10^{27} to over 10^{31} erg s^{-1} with occasional flares that can approach or exceed 1 $L_\odot$. A key feature of X-ray emission from YSOs is that it is highly variable. The launch of the XMM/Newton and Chandra (CXO) X-ray observatories has led to the detection of steady X-ray emission from shocks associated with HH objects.

Pravdo et al. (2001) detected X-ray emission from knot H in HH 2 in the HH 1/2 system in Orion. The emission region is compact (less than a few arcseconds) and arises from the fastest shocks in the entire HH 1/2 system. Proper motions (*Bally et al.,* 2002a) indicate velocities of over 400 km s^{-1}. Knot H is a high-excitation shock with strong [OIII] and radio continuum emission. This fast-moving feature is located near the axis of symmetry of HH 2 and may trace the location where a fast jet slams into much slower moving debris.

Favata et al. (2002) and *Bally et al.* (2003) detected the base of the HH 154 jet emerging from the L1551 IRS5 protobinary with XMM and CXO, respectively. The X-ray emission is offset from the location of the YSOs by about 0.5" along the jet axis. It is located close to the first 1.64 μm [FeII] knot at the base of the jet (*Pyo et al.,* 2002). The radial velocity of the [FeII] emission from the HH 154 jet extends to nearly 400 km s^{-1}. The X-ray spectrum implies a much lower column density of foreground hydrogen and dust in front of the X-ray source than the column density in front of IRS5 as determined from visual and IR extinction. Thus, the X-ray source is located near the base of the jet. *Bally et al.* (2003) proposed several models for the X-ray source including a collision front where the winds from each member of the IRS5 binary collide, a shock where the stellar wind impacts the disk surrounding the other member of the binary, or shocks formed where a wide-angle wind from one or both stars is/are collimated into a jet.

Both HH 2 and 154 are low-mass, low-luminosity protostars. *Pravdo et al.* (2004) found X-ray emission from HH 80/81, which is powered by a moderate-mass protostar with a much larger luminosity of order 10^4 $L_\odot$. As in the cases of HH 154 and HH 2, the X-ray emission is associated with the fastest components in this outflow.

Pravdo and Tsuboi (2005) found X-ray emission from the base of HH 168, the bright HH object associated with Cepheus A West powered by a cluster containing at least three early B stars in formation and a total luminosity of about 2×10^4 $L_\odot$. This feature coincides with the extended radio-continuum source HW at the base of HH 168. The plasma temperature is around $T_X \approx 6 \times 10^6$ K and the X-ray luminosity is around $L_X \approx 10^{29}$ erg s^{-1}.

Several additional HH objects or shocks may have been detected in the Orion Nebula by the COUP project (*Kastner et al.,* 2005), including HH 210, the fastest visually detected component of the shock-excited fingers of H_2 emission emerging from the 10^5 $L_\odot$ OMC1 cloud core located immediately behind the Orion Nebula. Of the more than 1000 X-ray sources found by COUP, a few appear to be associated with shocks at the bases of irradiated jets powered by young stars. *Raga et al.* (2002) have developed a simple, analytical model that can estimate the expected X-ray luminosity of an HH flow.

The detected X-ray-bright HH objects have plasma temperatures in the range $T_X = 10^6$–10^7 K. The X-ray spectrum is dominated by soft photons with energies below 1 keV. The soft-portion of the X-ray spectra are highly attenuated, implying column densities on the order of $\log N(H) = 10^{21}$–10^{22} cm^{-2}. The typical observed X-ray luminosities are around 10^{27} erg s^{-1}; this may be a severe lower limit on the intrinsic X-ray emission since most of the soft X-rays are absorbed by foreground gas and dust.

In summary, X-ray emission traces the fastest and highest excitation shocks in outflows. Most HH objects trace internal working surfaces where shock velocities are much lower than the flow velocities, indicating interactions between moving fluid elements. Thus, the majority of HH objects are dominated by emission in low-excitation tracers. X-ray emission indicates the presence of hard shocks that create high-excitation conditions with temperatures on the order of 10^6–10^7 K. Purely hydrodynamic shocks with speeds around 200–300 km s^{-1} can, in principle, produce such high temperatures. However, observations show that X-rays are only seen from HH objects with velocities larger than 300 km s^{-1} that tend to be associated with radio continuum emission. The absence of X-ray emission from shocks with speeds around 200–300 km s^{-1} indicates that postshock plasma temperatures are somewhat lower than expected from purely hydrodynamic shocks ramming stationary media consisting of a cosmic mixture of hydrogen and helium. It is possible that the hard, X-ray emitting shocks are also propagating into moving media or that postshock temperatures are lowered by other mechanisms such as the addition of coolants or very strong magnetic fields. Grains entering the X-ray emitting volume can radiate away the energy imparted by impacting electrons. Sputtering of these grains can poison the X-ray plasma by injecting metals with tightly

bound inner K- and L-shell electrons, which act as efficient coolants.

2.2. Ultraviolet Results

The Space Telescope Imaging Spectrograph (STIS) was used to observe a number of young stars and their HH objects. *Grady et al.* (2005) detected outflows and disks in the immediate vicinity of several Herbig AeBe (HAeBe) stars. *Devine et al.* (2000b) discovered a bipolar jet, HH 409, from the HAeBe star HD 163296 in the Lyman α line. *Grady et al.* (2004) report a bipolar microjet, HH 669, from the bright HAeBe star, HD 104237 (DX Cha). The age of this star, and the small association of young stars around it, has been estimated to be around 5 m.y. A growing number of low mass-loss-rate outflows emerge from stars with ages of several million years. The Lyman α observations are especially sensitive to the very low mass-loss rates of these older YSOs.

Hartigan et al. (1999) obtained UV spectra of HH 46/47 with HST, finding emission from a large number of permitted resonance lines and forbidden transitions. Comparison with shock models indicates a large range of excitation conditions.

Over a dozen proplyds, young stars, and irradiated jets in the Orion Nebula have been observed by STIS at both visual and UV wavelengths. The visual-wavelength STIS observations provide much better spatial resolution than groundbased spectroscopy. With a 0.1" slit, the spectrum of the proplyd ionization front, photo-ablation flow, stellar jet, and star can be spatially resolved. Many of Orion's irradiated microjets exhibit strong kinematic asymmetries in which the brighter jet beam has a lower radial velocity than the fainter counter-jet beam (see section 3.4). The HH 514 microjet emerging from the proplyd HST2 provides an excellent example (Fig. 1) (*Bally et al.,* 2006). This behavior is similar to that of many other irradiated jets and will be discussed further below.

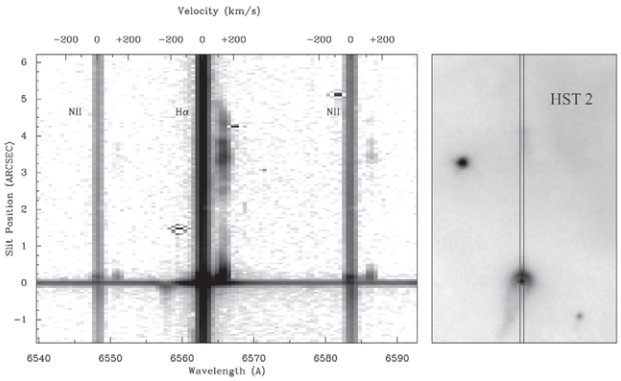

Fig. 1. (Left) A long-slit spectrum showing Hα and the [NII] doublet from the HH 514 microjet obtained with STIS on HST. (Right) An HST/WFPC2 F656N (Hα) image showing a direct image of the proplyd HST2 (170–337), the source of the HH 514 jet. The orientation and relative size of the STIS slit used to obtain the spectrum is shown. From Smith et al. (in preparation).

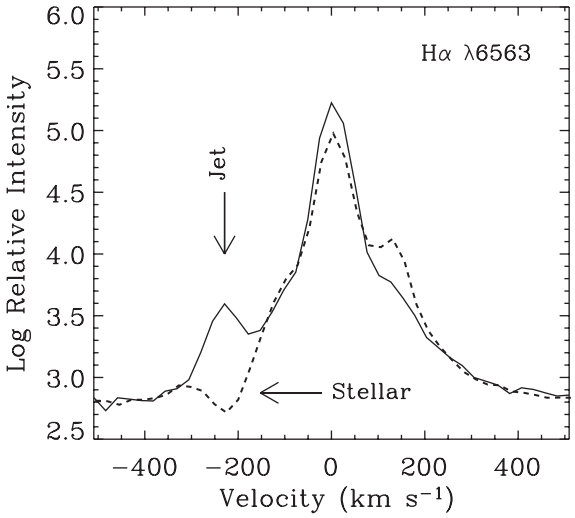

Fig. 2. The solid line shows the STIS spectrum of the Hα emission line profile about 0.2" south of the star in HST2 showing the blue-shifted emission associated with the southern lobe of the HH 514 jet. The dotted line shows the STIS spectrum of the Hα emission line from the central star in HST2 (170-337). Note the absorption feature at the velocity of the blue-shifted lobe of the HH 514 jet. From Smith et al. (in preparation).

A remarkable aspect of the HH 514 jet and source star is the presence of a dip in the stellar Hα emission line profile with exactly the same radial velocity and line width as the HH 514 counterjet at positions offset from the central star (Fig. 2). It is possible that the intense Lyman α radiation produced in the Orion Nebula, combined with self-irradiation by the central star in the proplyd, pumps the n = 2 level of hydrogen near the base of the jet. This process requires a very high density neutral envelope [$n(H) > 10^5$ cm^{-3}]. Thus, at the base of the HH 514 jet, the n = 2 level may be sufficiently populated by trapped Lyman α to enable absorption in the 6563 Å (n = 2–3) Hα line. The presence of an absorption dip at the velocity of the HH 514 counterjet implies that the outflow is launched as a wide-angle wind with an opening angle at least as large as the inclination angle of the jet. After producing the absorption, the wind is funneled into the highly collimated jet that propagates for tens of arcseconds to the south.

Unfortunately, the loss of STIS has brought UV and high-angular-resolution (0.1") visual wavelength studies of protostellar outflows to an end for the time being.

3. VISUAL WAVELENGTH SURVEYS

3.1. Wide-Field Surveys: Counting Shocks and Determining the Impact of Outflows

The continuing development of large format arrays in the visual and near-IR has enabled the first complete surveys of entire giant molecular clouds and star-forming complexes

with narrow-band filters sensitive to selected shock tracers. Visual wavelength imaging complements spectral line surveys at IR, submillimeter, millimeter, and radio wavelengths.

Narrow-band Hα, [SII], and H_2 imaging of entire GMCs and star-forming complexes provide unbiased samples of shocks and their associated outflows. Such data are an excellent way to find new YSOs and outflows. They have been used to estimate the contribution of outflows and shocks to the generation and sustenance of chaotic, turbulent motions, and the momentum and energy budgets of molecular clouds. Wide-field Hα and [SII] imaging has been the best way to identify giant, parsec-scale outflows. In this section, we first summarize recent or ongoing surveys, highlighting the Perseus cloud as a specific example, then we review recent developments in the study of giant outflows, and finally discuss recent visual-wavelength observations of irradiated jets in HII regions.

3.2. Narrow-Band Surveys

Nearby (d < 1 kpc) clouds surveyed in one or more narrow-band filters at visual wavelengths include NGC 2264 (*Reipurth et al.,* 2004), S140 (*Bally et al.,* 2002b), Perseus (*Walawender et al.,* 2005), Orion A and B (*Bally et al.,* 2002c; Bally et al., in preparation), Taurus, Ophiuchus, Serpens, Chamaeleon I, Circinus, NGC 7000, and portions of Cepheus. Many of these datasets remain unpublished because the complete analysis has proven to be labor intensive. *Phelps and Barsony* (2004) and *Wilking et al.* (1997) presented CCD surveys of the entire ρ-Oph dark cloud, finding several dozen HH objects on the surface of this cloud. *Khanzadyan et al.* (2004a) surveyed these clouds in H_2. The Orion A molecular cloud was surveyed in its entirety in H_2 by *Stanke et al.* (1998, 2000, 2002).

Hundreds of individual shock systems in dozens of outflows and jets, many with parsec-scale dimensions, were found. A deep narrow-band CCD survey of both Orion A and B detected hundreds of HH objects including several dozens of parsec-scale HH flows, and a remarkable chain, nearly 2.5° long, terminating near HH 131 from a suspected source in or near the L1641N cluster (*Reipurth et al.,* 1998b; Bally et al., in preparation).

Walawender et al. (2005) used the Kitt Peak Mayall 4-m reflector to completely image the entire Perseus molecular cloud in Hα, [SII], and broadband SDSS I'. This work resulted in a reevaluation of energy and momentum injected into the cloud by outflows. The origin of the random motions, turbulence, and cloud structure was previously discussed by *Miesch and Bally* (1994), *Miesch et al.* (1999), and *Bally et al.* (1996). *Walawender et al.* (2005) compared the energy and momentum traced by these shocks with the total turbulent kinetic energy and momentum in the Perseus clouds as traced by CO observations. Walawender et al. also analyzed the amount of energy and momentum injected by molecular outflows. The results of these preliminary analyses can be summarized as follows: Outflows inject more than sufficient energy and momentum to drive turbulence motions and even to disrupt individual cloud cores such as NGC 1333. For example, *Bally et al.* (1996) found that in the NGC 1333 region, there are dozens of currently active outflows. If this level of activity is typical, then in a steady state the mean time between the passage of a shock with sufficient speed to dissociate molecules in any random parcel of gas is about 10^4–10^5 yr. Thus, outflows can self-regulate star formation and even disrupt surviving portions of the cloud core in regions such as NGC 1333. However, on the scale of the entire 10^4 $M_\odot$ GMC, outflows may fail by nearly an order of magnitude to resupply the momentum being dissipated by the decay of turbulent energy. Thus, while being able to self-regulate star formation on the scale of individual cloud cores containing a few hundred solar masses, outflows may not supply the random motions observed on large scales. To maintain a steady state, other sources of energy are required. Possible sources include acceleration of the cloud by soft-UV photo-heating, ionization of the cloud by hard-UV radiation, the impacts of winds from massive stars and supernova explosions, or the injection of turbulent energy from large-scale flows such as superbubbles, or collisions with other clouds.

Noteworthy results from the Perseus imaging survey include the discovery of a giant flow, HH 280/317/492/493, emerging from the head of the cometary cloud L1451 (*Walawender et al.,* 2004). This cloud has apparently been sculpted by UV radiation from the B0 star 40 Per located over 25 pc away. The outflow propagates through a portion of the Perseus cloud sufficiently transparent to reveal background galaxies, impacts the western edge of the L1455 cloud at HH 317D, and forms an obscured H_2 emitting shock. The deflected flow powers the HH object HH 317.

Perhaps the richest source of HH jets and outflows within 400 pc of the Sun is the NGC 1333 region in Perseus (*Bally and Reipurth,* 2001; *Bally et al.,* 1996) (see Fig. 3). Bent jets, giant flows, and H_2 shocks overlap along the line of sight, and on deep images are essentially confusion limited. The HH 7/11 group traces a collimated flow emerging from a dense cloud core at roughly PA ~ 125° and originates from the vicinity of an embedded Class I source, SVS 13 (*Strom et al.,* 1976). However, *Rodríguez et al.* (1997, 1999) found several additional embedded radio sources that cluster around SVS 13. The HH 7/11 group is embedded within a high-velocity CO outflow (*Knee and Sandell*, 2000; *Rudolph et al.,* 2001). This flow is one of the few that has been detected and mapped in the 21-cm line of HI (*Lizano et al.,* 1988; *Rodríguez et al.,* 1990). The HH 7/11 region turned out even more complex with the detection of additional nearby sources; the radio source VLA 20 (*Rodríguez et al.,* 1999) and the Class 0 protostar SVS 13B, which is known to drive a highly collimated molecular outflow along a roughly north-south direction (PA ~ 170°) (*Bachiller et al.,* 1998). This flow is bright in the shock-enhanced tracer, SiO. The radio studies of *Rodríguez et al.* (1999) show that the SVS 13 region contains a 3' long chain of over a dozen radio continuum sources that are embedded in a ridge of dense molecular gas and submillimeter cores extending along PA ~ 20°

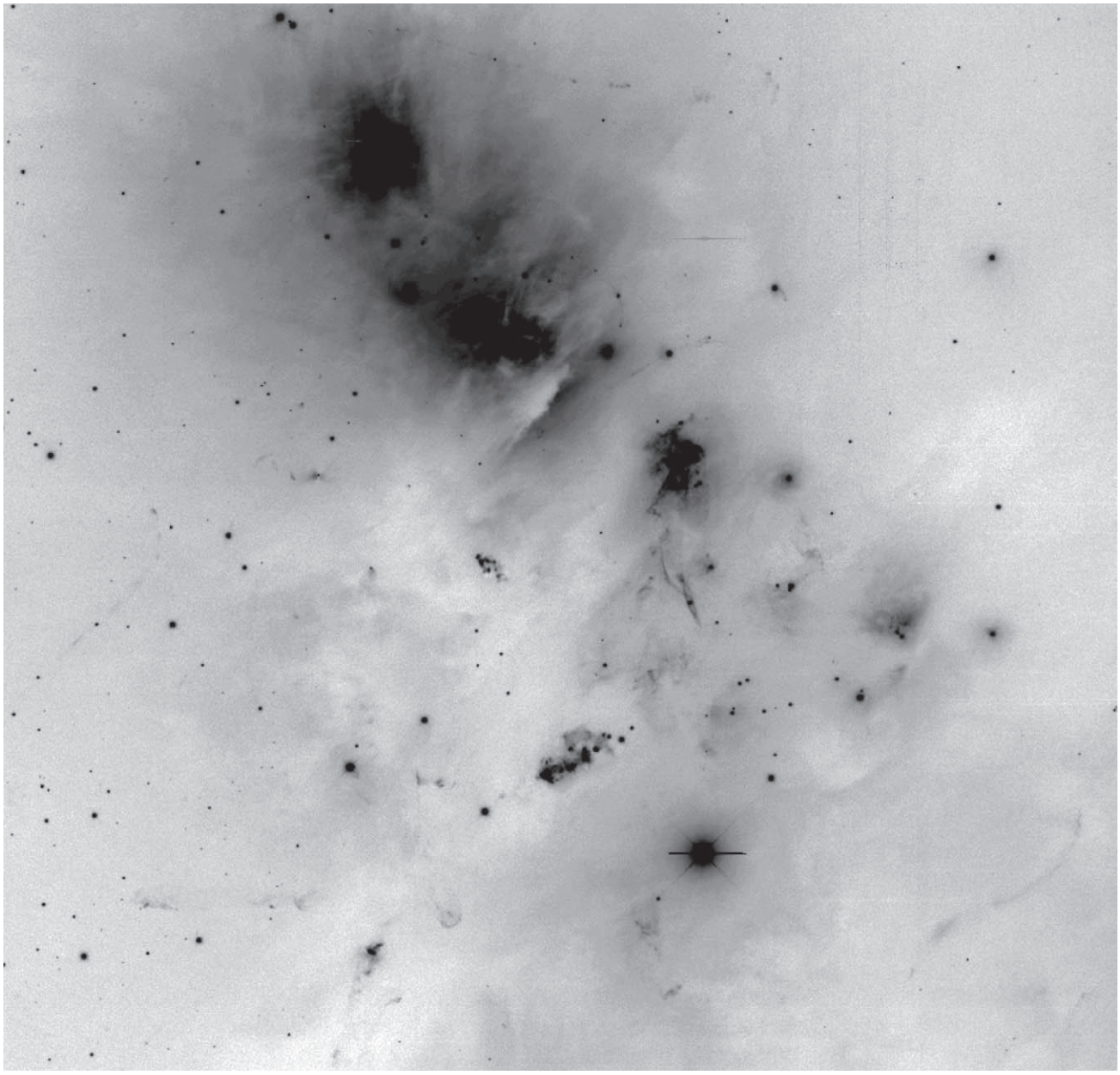

Fig. 3. The NGC 1333 region seen in the combined light of Hα and [SII]. Images obtained with the Mosaic prime-focus camera on the Mayall 4-m reflector.

(*Hatchell et al.,* 2005). The 40"-long dense core containing SVS 13 (VLA 4) includes VLA 20, VLA 3, VLA 17 (also known as SVS 13B), and VLA 2 [H_2O (B)]. Thus, it is perhaps not surprising that multiple outflows originate from this region. Interferometric millimeter-wave observations by *Bachiller et al.* (2000) have provided evidence that the actual driving source of the HH 7/11 outflow is indeed SVS 13. These authors produced high-resolution CO maps that show that SVS 13 is the point of origin of a high-velocity CO flow oriented toward HH 7/11.

Other noteworthy regions in Perseus include Barnard 4, which contains the HH 211 jet and is now known to be the site of a small cluster of embedded stars, and dozens of H_2 shocks (*Eislöffel et al.,* 2003) and HH objects (*Walawender et al.,* 2005). Barnard 1 in the central portion of Perseus (*Walawender et al.,* 2005) has also been proven to be a rich source of outflows, some of which are parsec-scale.

3.3. Giant Outflows

Bally and Devine (1994) found the first parsec-scale outflow from a low-mass star by recognizing that the HH 34 jet was merely the innermost part of a giant flow extending to HH 33/40 in the north and HH 87/88 in the south. This association was confirmed by *Devine et al.* (1997). Many more giant outflows were reported by *Ogura* (1995),

Reipurth et al. (1997), and *Eislöffel and Mundt* (1997). Most well-studied HH objects have turned out to be internal working surfaces within much larger parsec-scale giant protostellar outflows. These flows include the 10-pc-long HH 111/113/311 system in the northern portion of Orion B, the HH 1/2/401/402 system in Orion A, the HH 83/84 system on the west side of the Orion A cloud, and several nearly 10-pc-long chains emerging out of the L1641N cluster in Orion A (*Reipurth et al.,* 1998b). Since the late 1990s, dozens of giant, parsec-scale outflows have been found.

One of the nearest sites of ongoing star formation in Taurus, the L1551 cloud, has continued to reveal many surprises. In addition to the X-rays at the base of the HH 154 jet emerging from IRS5 (see above), this region contains criss-crossing jets, parsec-scale HH flows, a common CO outflow lobe inflated by several sources, and jet/wind interactions. Multiepoch images were used by *Devine et al.* (1999) to measure proper motions, which revealed that the L1551 bipolar CO outflow is powered not just by the twin jets from L1551 IRS5, but also by a highly collimated jet, HH 454, emerging from one component of the L1551NE binary located about 1' east of IRS5. Thus, the L1551 CO outflow lobes are collectively inflated by winds and jets from several individual protostars. Devine et al. noted that the bright shock HH 29 and possibly HH 28 in the blue-shifted lobe of the L1551 CO outflow, together with components of HH 262 in the red-shifted CO lobe, lie exactly on the axis of HH 454 emerging from L1551NE, making this object the likely driving source. HST imaging of HH 29 by *Devine et al.* (2000a) provide supporting evidence for this hypothesis. A large but faint bow shock, HH 286, lies 10' beyond the edge of the L1551 molecular cloud and the red-shifted lobe of the main L1551 molecular outflow in a region full of background galaxies, indicating that the flows from IRS5 and NE have blown completely out of the L1551 cloud. Thus, L1551 contains a remarkable, giant outflow energized by multiple sources.

Pound and Bally (1991) found a remarkable 30' long red-shifted outflow lobe that extends due west from HH 102. Although a component of L1551NE has been proposed as a driver, it is possible that there are additional highly embedded YSOs, or previously unrecognized companions to known YSOs near NE and IRS5, that are responsible for this outflow lobe.

The famous HH 30 jet in the L1551 cloud was also found to extend many arcminutes northeast of HL and XZ Tau in the L1551 cloud and to cross the lobes of the L1551 IRS5/NE common outflow lobe toward the southwest. Each of the well-known T Tauri stars in the cloud, HL and XZ Tau and LkHα 358, appears to power an outflow in its own right. Recent integral field spectroscopy and proper motion measurements by Magakian et al. (in preparation) provide evidence that the HL Tau jet is being deflected by a wide-angle wind from XZ Tau. These authors also hypothesize that a collimated outflow from LkHα 358 is deflected by the southwestern lobe of the XZ Tau wind to produce the "Hα" jet a few arcseconds southeast of HL Tau. It is remarkable that the small, roughly 40-$M_\odot$ L1551 cloud contains about a dozen active outflows, several of which have clearly blown out of the parent cloud and are powering shocks beyond the extent of the associated CO outflow lobes.

The well-known HH 46/47 jet was discovered to be merely the inner part of a giant outflow injecting energy into the interior of the Gum Nebula by *Stanke et al.* (1999), who discovered a pair of giant bow shocks, HH 47NE and HH 47SW, over 10' from the HH 46/47 jet, making this well-studied object a member of the class of giant flows.

Bally et al. (2002c) found that the chain of HH objects HH 90 through 93 located in the Orion B cloud north of NGC 2024 form a single giant flow from the 10 $L_\odot$ Class I source IRAS 05399-0121. This is one of the first results of the complete narrow-band survey of the Orion A and B cloud discussed above.

One of the most remarkable giant bow shocks near a star-forming region is the 30' wide Hα bow shock surrounding HH 131 (*Ogura,* 1991; *Wang et al.,* 2005). The most remarkable aspect of HH 131 and the surrounding filamentary nebula is that it is located more than a full degree from the nearest edge of the Orion A molecular cloud. *Stanke* (2000) hypothesized that the chain of H_2 features emerging from source S3 in the southern portion of the Orion A cloud may trace the parent flow leading to HH 131. However, there are no intervening HH objects, and the orientation of the giant bow shock surrounding HH 131 suggests a source located toward the north. The narrow-band imaging survey of Orion has led to the identification of a chain of faint bow shocks and [SII]-bright filaments extending from the vicinity of V380 Ori and the L1641 cluster about 2° north of HH 131. *Wang et al.* (2005) suggest that HH 131 originated from the vicinity of the L1641N cluster. If so, then HH 131 may be the southern end of a giant flow from this cluster, which contains HH 403–406 in the north (*Reipurth et al.,* 1998b), and may contain HH 61/62/127/479/480, which lie south of L1641N between it and HH 131. If these shocks exhibit similar radial velocities and if their proper motions point toward HH 131, then this system may represent the largest giant flow found to date.

Not all shocks in star-forming regions are protostellar. The Rosette Nebula contains a set of high-excitation arcs of emission that have the morphology of bow shocks. They form a linear chain extending across the nebula from northeast to southwest. Tracing this orientation back toward the apparent source of these shocks, there are no known IRAS sources or protostars. However, this direction does contain a supernova remnant — the Monoceros N-ring — that is impinging on the outskirts of the Rosette Nebula. It is possible that outlying portions of the expanding supernova debris field energize the Rosette features, which are rendered visible by the intense UV radiation of the Rosette's massive stars.

Reipurth (2000) noted that most sources of prominent HH flows in low- to moderate-mass star-forming regions are members of multiple systems. He hypothesized that disk perturbations produced during close approaches of compan-

ion stars trigger the most energetic episodes of mass loss. As non-hierarchical multiples evolve toward hierarchical systems consisting of a tight binary and either a distant companion or an ejected star, unusually strong outbursts of outflow activity occur. Reipurth postulated that such dynamical interactions produce the giant, parsec-scale outflows, which therefore form a fossil record of the dynamical evolution of newborn binaries. In this picture, the FU Ori outbursts occur at the end of jet production, when the binary companion gradually destroys the magnetic anchoring in the inner disk that is required for jet launch and collimation (*Reipurth and Aspin,* 2004).

3.4. Irradiated Jets

The discovery of irradiated jets embedded in HII regions and in UV-rich environments (*Reipurth et al.,* 1998a; *Cernicharo et al.,* 1998; *Bally and Reipurth,* 2001) has flowered into a productive area of research. Irradiated outflows permit the measurement of flow properties using the standard theory of photo-ionized plasmas that can provide a more robust method of density measurement than the analysis of the highly nonlinear theory of shocks. External radiation renders visible much weaker jets and outflows than the flows seen in dark clouds, where only shock-processed gas can be seen at visual and near-IR wavelengths.

A group of irradiated jets, HH 444 to 447, were found about 20' west of the Horsehead Nebula in Orion in the σ Ori cluster (*Reipurth et al.,* 1998a). These four outflows are located within about 10' of the massive O9.5 star σ Ori in a region that contains no molecular gas and very little extinction. The brightest jet, HH 444, is highly asymmetric in intensity and radial velocity. The brighter jet beam, which faces away from σ Ori, is at least four times brighter and has a radial velocity about two times slower than the faint counter jet. A pair of Hα bow shocks are visible about 1' from the source star. The other three irradiated jets in the σ Ori cluster exhibit similar asymmetries. In all cases, the brighter jet beam is slower and faces away from the illuminating star σ Ori. *Reipurth et al.* (1998a) noted an anomalous jet-like tail emerging from the source star of HH 445 but at about a 20° angle with respect to the actual jet. The Hα images show that this 10" long feature points directly toward σ Ori and that it tapers to an unresolved tip away from the source of HH 445. HH 444 and HH 447 also exhibit similar, but fainter tails whose morphology resembles the proplyds observed in the Orion Nebula. *Andrews et al.* (2004) presented high-resolution long-slit spectra of several of these jets obtained with the HIRES spectrometer at the Keck Observatory. These spectra show that, within 2" of the source star of HH 444, the main jet contains two converging radial velocity components (Fig. 4). The first branch starts near the star with a large negative radial velocity (similar to the faint counter jet, but with the opposite sign), decelerates, and merges with a second, brighter branch that starts near the star with a very low radial velocity and accelerates to join with the high-velocity branch. After the two

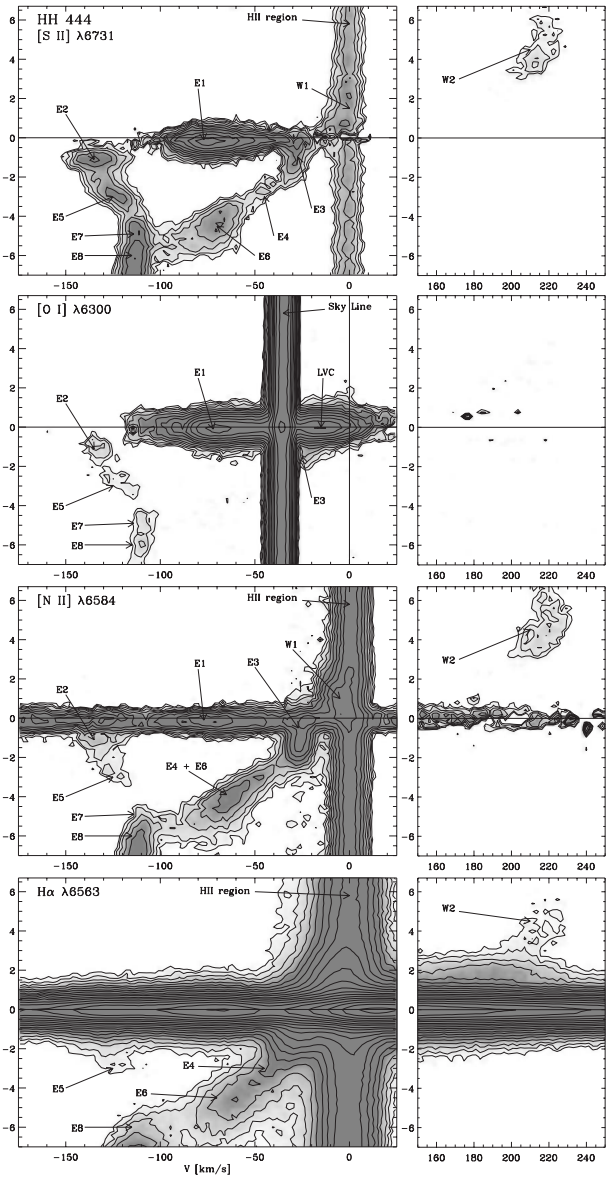

Fig. 4. High-resolution long-slit spectra showing different lines of the irradiated HH 444 jet. The jet is seen in the panels to the left, and the faint counter jet in the righthand panels. From *Andrews et al.* (2004).

branches merge, the radial velocity remains constant for many tens of arcseconds.

A likely interpretation of HH 444 is that the source star is surrounded by a dense, but compact, circumstellar envelope or disk. The jet pointing away from σ Ori interacts with an arcsecond-scale cavity in the envelope and entrains some material from it. The flow may be brightest where it interacts with and entrains material from the walls of a cavity in the envelope. The nearside of the interaction zone may be traced by the first, decelerating, branch of the HH 444 jet, while the farside may be traced by the accelerating second branch seen in the Keck HIRES spectra. The counterjet may not interact significantly with circumstellar matter, is

not decelerated, and does not show merging branches of emission. UV-induced photo-ablation of the circumstellar environment by σ Ori may have removed any such medium on this side of the circumstellar disk. Thus, the observed asymmetries in the irradiated jets may be a result of interactions with a highly asymmetric circumstellar environment.

During the last five years, many more irradiated jets have been discovered in the Orion Nebula and in NGC 1333 (*Bally and Reipurth,* 2001; *Bally et al.,* 2006), in M43 (*Smith et al.,* 2005), in the NGC 1977 cluster about 0.5° north of the Orion Nebula (Bally et al., in preparation), in the Carina Nebula (Smith et al., in preparation), and in some other regions. Many of these jets exhibit asymmetries similar to the σ Ori jets.

However, a number of additional features have emerged. A significant subset of irradiated jets show extreme bends indicating deflection by a side wind, radiation pressure, or the rocket effect. The subarcsecond resolution of HST was required to identify dozens of irradiated jets in the core of the Orion Nebula (*Bally et al.,* 2000). Some, such as HH 514 emerging from the proplyd HST 2, exhibit pronounced kinematic and intensity asymmetry. HH 508, emerging from one of the four companion stars to θ^1 Ori B, the northern member of the Trapezium, is a one-sided microjet that has the highest surface brightness of any HH object in Hα, probably due to its location within 10^3 AU from an OB star. *Bally et al.* (2000) and *Bally and Reipurth* (2001) noted that about a dozen low-mass stars, located mostly in the southwestern part of the Orion Nebula, were surrounded by parabolic arcs of emission, indicating deflection of circumstellar material away from the nebular core. These were dubbed "LL Ori" objects after the prototype LL Ori (Fig. 5), which was first noted by *Gull and Sofia* (1979) to be a possible example of a wind-wind collision front. The system HH 505 contains both a jet and an LL Ori bow shock. *Masciadri and Raga* (2001) modeled the parabolic bow as a jet deflected by a side wind. They were able to reproduce the Hα morphology of the parabolic bow surrounding HH 505 and its source star, showing that the bow is produced by the weak shocks formed where the side wind interacts with the jet material that moves away from the jet axis after passing through the bow shock at the head of the jet.

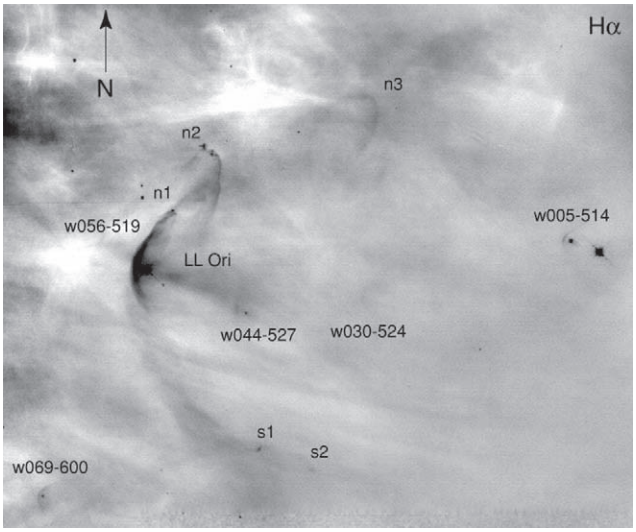

Fig. 5. An HST/WFPC2 image showing Hα emission from the parabolic bow shock and compact bow shock surrounding LL Ori in the Orion Nebula. The deflected jet is invisible in this image, but can be seen as a high-velocity feature in Fabry-Perot data cubes.

The Advanced Camera for Surveys (ACS) on HST revealed dozens of additional irradiated outflows in the outskirts of the Orion Nebula (*Bally et al.,* 2006). Some of the larger outflows, such as HH 503 to 505, were previously detected on groundbased images (*Bally and Reipurth,* 2001), but many consist of subarcsecond chains of knots and compact bow shocks lost in the glare of the nebula on groundbased images. The ACS images show that the jets in many of these outflows consist of a fine series of subarcsecond knots whose proper motions can be measured on HST images taken only a year apart. The inner parts of these flows show proper motions of up to 300 km s^{-1}. The jets tend to fade to invisibility at distances ranging from less than 1 to 10" from the source to be replaced, in some flows, by a series of bow shocks. HH 502 in the southern part of the Orion Nebula is a clear example. This arcminute-scale flow has a long southern lobe containing a half-dozen bow shocks while the shorter northern lobe contains three. The flow exhibits bending away from the nebula core.

The ACS images demonstrate that many LL Ori objects, including LL Ori itself, contain jets that are frequently asymmetric. In some outflows, such as HH 505, proper motions show that jet segments are deflected away from the nebular core as they skirt along the parabolic bow that wraps around the source star and bipolar jet. *Bally et al.* (2006) show that while most LL Ori-type bows and bent jets in the southwestern quadrant of the Orion Nebula may be deflected by a large-scale outflow of plasma from the nebular core, even in the absence of such a side wind, radiation pressure acting on dust and the asymmetric photo-ablation of a neutral jet beam can also deflect irradiated jets. As the neutral jet beam emerges from the neutral circumstellar environment into the irradiated environment of the HII region interior, the photo-ionized skin of the jet expands away from the remaining neutral jet core. Because for most irradiated jets, the radiation field is highly anisotropic, the photo-ablation flow exerts a force on the neutral jet beam, deflecting it away from the illuminating star or stars.

The jet densities, mass-loss rates, and other properties can be estimated from the jet proper motions or radial velocities combined with estimates of the electron density at the jet surface determined from the [SII] line ratio, the Hα emission measure, or the apparent length of the jet (*Bally et al.,* 2006). Analysis of the irradiated jets in the Orion Nebula indicate mass-loss rates ranging from as little as 10^{-9} $M_\odot$ yr^{-1} to more than 10^{-7} $M_\odot$ yr^{-1}. Observations of irradiated jets can detect lower mass-loss rates than the classical methods used to study outflows such as CO, radio continuum, or the various shock-excited tracers.

A particularly beautiful example of a jet powered by a low-mass young star embedded in a circumstellar disk and a large externally ionized proplyd was presented by *Bally et al.* (2005). The Beehive proplyd contains a several hundred AU diameter silhouette disk, a jet that can be traced for over 1' south of the source star in Fabry-Perot images, and a chain of large bow shocks, HH 540, visible on ground-based images. The proplyd ionization front contains a set of three or four concentric rings of enhanced Hα emission that appear as corrugations. These features may have been triggered by a series of mass ejections from the central star that are responsible for some of the bow shocks in the HH 540 outflow.

The Orion Nebula contains at least several giant, low radial velocity bow shocks best traced by [SII] Fabry-Perot data (*Bally et al.,* 2001). The HH 400 bow is about 2' in diameter, 8' long, and extends south from a few arcminutes south of the Bright Bar in the Orion Nebula. The bow orientation indicates that the source lies somewhere in the general vicinity of the Trapezium stars. It could be a star still embedded in one of the molecular cloud cores behind the nebula.

The Hα and [SII] survey of the entire Orion A and B clouds conducted with the NOAO 4-m telescopes and their mosaic CCD cameras (Bally et al., in preparation) reveal the presence of a 5' scale bow shock at the southwestern periphery of the Orion Nebula. This feature may be the terminus of a 30' scale outflow that emerges from the Orion Nebula core parallel and just north of Orion's Bright Bar. Many filaments and arcs of Hα emission located south and southwest of the Orion Nebula core may trace shocks or dense photo-ionized filaments in this flow. Multiepoch HST images show proper motions ranging from 20 to over 50 km s^{-1}. This large-scale flow may be several times larger than HH 400. HH 400 and this giant flow in the southwestern part of the nebula may be responsible for deflecting the bent jets and LL Ori-type bows in this quadrant of the nebula. However, it is not clear if this is a giant outflow driven by one or more embedded young stars, the leading edge of the stellar wind bubble powered by the Trapezium stars, or possibly the outflow of plasma photo-ablated from the background Orion A cloud by the Trapezium stars.

Although the nature of the giant bow shocks emerging from the Orion Nebula remains unclear, protostellar outflows have been observed to break out of their parent molecular clouds into adjacent HII regions where they become irradiated and ionized. Examples include a pair of giant bow shocks emerging into the S140 HII region from the adjacent dense cloud core (*Bally et al.,* 2002b), the quadrupolar outflow containing HH 124 and HH 571/572 from NGC 2264N (*Ogura,* 1995; *Reipurth et al.,* 2004), and the giant bow shocks emerging from embedded sources in the dense cloud cores associated with IC 1396N (*Reipurth et al.,* 2003).

Smith et al. (2004) reported the discovery of several parsec-scale irradiated outflows emerging from dusty pillars embedded within the Carina Nebula located at a distance of about 2.2 kpc (Fig. 6). The HH 666 flow emerges from a moderate luminosity IRAS source, drives a jet bright in [FeII], Hα, and [OIII], and is associated with a series of giant bow shocks. Long-slit spectra reveal a set of three distinct Hubble flows indicating a series of three ever older mass ejections that exhibit radial velocities as large as ±200 km s^{-1}.

The Carina Nebula also contains many small cometary clouds with sizes up to tens of thousands of AU in length. Many contain IR sources, presumably young stars in their heads. A few exhibit spectacular irradiated jets that are very bright in Hα, presumably because the UV and ionizing radiation field in Carina is nearly 100× stronger than the field in the Orion Nebula. The presence of cometary clouds with properties similar to Orion's proplyds that contain IR sources or visible stars in their heads and irradiated jets and outflows indicates that active star formation is still occurring within the molecular clouds embedded in and surrounding the Carina Nebula HII region.

4. INFRARED OBSERVATIONS OF MOLECULAR JETS

4.1. H_2 and [FeII] as Tracers of Jets and Bow Shocks

The 1990s saw a rapid increase in near-IR observations of outflows, particularly flows from embedded Class 0 and Class I YSOs (see the review by *Reipurth and Bally,* 2001). Observations benefited in particular from increasing array sizes and improved image quality at 4-m-class telescopes. Between 1 and 2.5 μm the most useful probes of outflows are undoubtedly H_2 and [FeII]. Both species produce a wealth of lines across the near-IR bands that allow us to measure the excitation and kinematics of shocked gas in outflows. H_2 in particular is also proving to be a powerful tracer of parsec-scale jets (*Eislöffel,* 2000; *Stanke et al.,* 2002) (see also Fig. 7) as well as outflows from massive (early-B-type) young stars (Fig. 8) (Varricatt et al., in preparation).

Rigorous efforts have been devoted to interpreting H_2 (and CO) observations of jets in terms of entrainment of ambient gas (e.g., *Downes and Cabrit,* 2003) and the physics of discrete shock fronts (e.g., *Smith et al.,* 2003a). *Rosen and Smith* (2004) claim that the H_2 1-0 S(1)/CO J = 1–0 flux ratio may even be used as an age discriminant. Although collimated jets seem present at all evolutionary stages, from Class 0 through to optically visible TTSs, there are still cases where poorly collimated winds best explain the observations (*Lee et al.,* 2001; *Davis et al.,* 2002). Whether collimation is a factor of age or environment is not yet clear.

For individual shock features, line profiles — when combined with maps of excitation across the shock surface — can be used to constrain bow shock physics, as well as parameters pertaining to the overall outflow, such as the transverse magnetic field strength, jet density, velocity, and flow orientation (*Davis et al.,* 2001a; *Schultz et al.,* 2005). Typically, magnetically cushioned C-type shocks are required to produce the bright molecular emission in extended bow wings, while dissociative J-type shocks probably produce

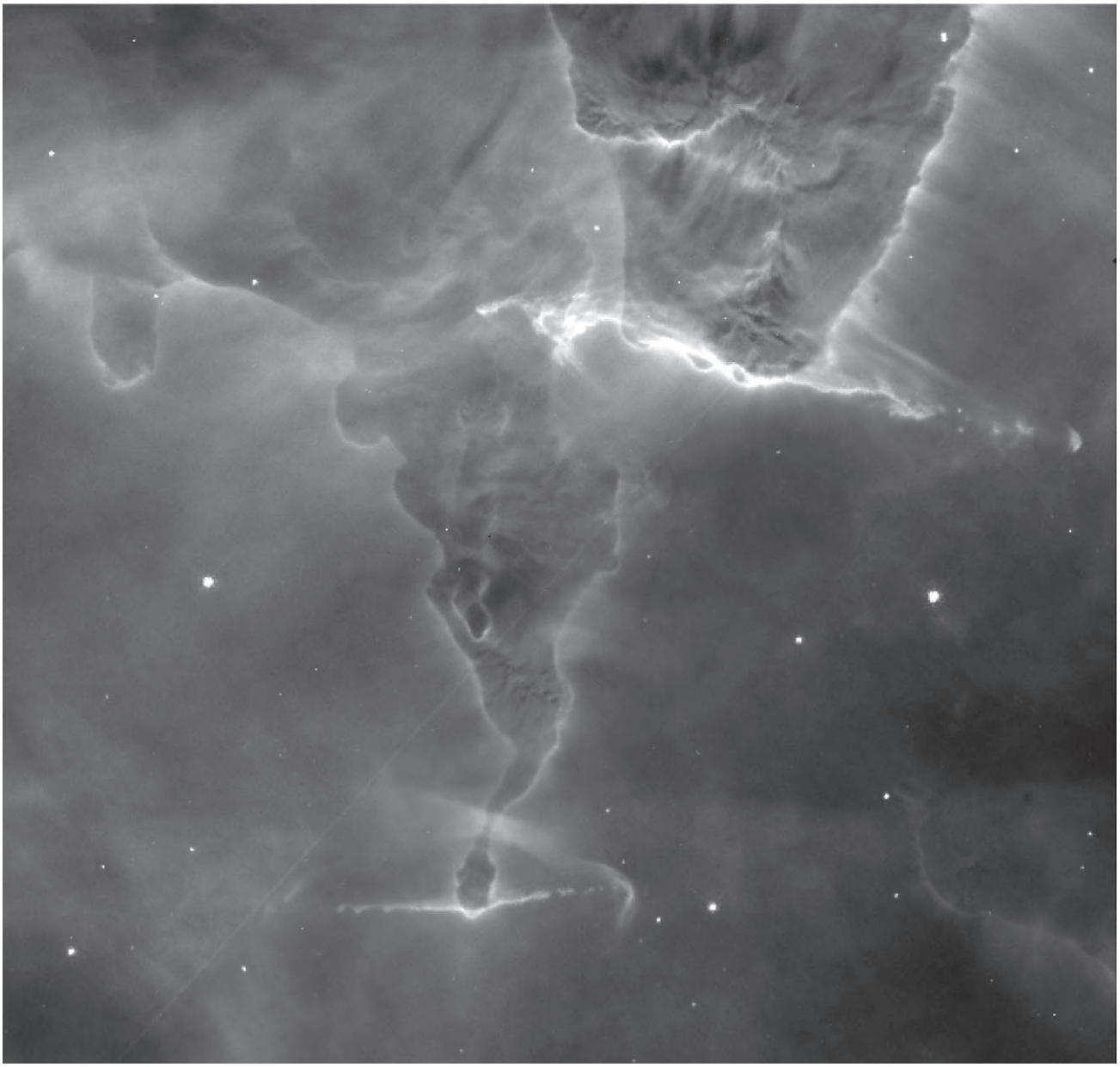

Fig. 6. A pair of bright externally irradiated jets emerging from dusty pillars north of the cluster Trumpler 14 in the Carina Nebula observed with ACS on HST with the F658N filter, which transmits Hα and [NII]. From Smith et al. (in preparation).

the [FeII] emission near the bow head (*O'Connell et al.,* 2005). Fluorescent excitation, which produces a lower rotational than vibrational temperature in H_2 excitation diagrams, can be ruled out in most cases.

In some flows, however, enhancement of molecular emission from levels at very low and very high excitation, which can be difficult to reproduce with steady-state J- and C-type shocks, respectively, have lead researchers to consider the intermediate case of a J-type shock with a magnetic precursor (e.g., *McCoey et al.,* 2004; *Giannini et al.,* 2004). Such a structure is possible only if there is a sufficiently-strong magnetic field, so that the J shock is enveloped by a C-type flow. Indeed, given the lengthy timescale for a shock wave to attain steady state (~10^5 yr), a J shock may slowly evolve into a C shock (via a J shock plus magnetic precursor) over the lifetime of an outflow, requiring nonequilibrium shock modeling of bows in some regions (*Le Bourlot et al.,* 2002; *Flower et al.,* 2003). This also means that younger flows may drive shocks that are closer to J than C type, with correspondingly higher excitation spectra and molecular line populations closer to LTE.

Parabolic bow shapes, preshock densities of 10^4–10^5 cm^{-3}, and shock velocities (relative to the preshock medium) of 30–100 km s^{-1} generally best describe the observations (e.g., *Smith et al.,* 2003a; *Khanzadyan et al.,* 2004b; *Giannini et al.,* 2004). Inclined magnetic fields or an inhomogeneous preshock medium can produce asymmetries in observed bow shock shapes. It also seems clear that the jet itself must

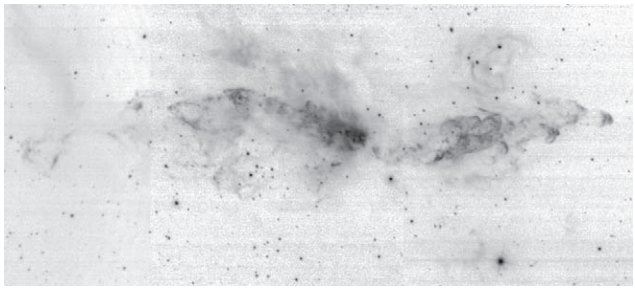

Fig. 7. The complex Cepheus A outflow in H_2. This image was obtained with the NICFPS camera on the 3.5-m Apache Point Observatory telescope in November 2004.

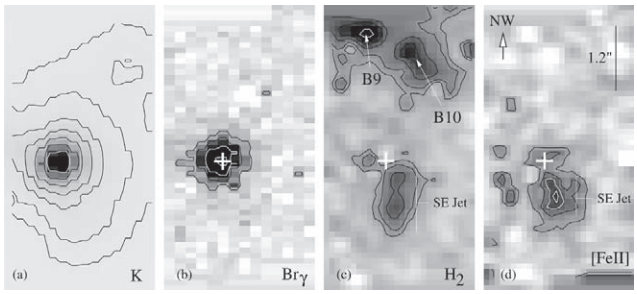

Fig. 8. Near-IR images extracted from UKIRT/UIST Integral Field spectroscopy data (*Davis et al.,* 2004). **(a)** The K-band image (2.03–2.37 μm) shows the nebulosity associated with the massive YSO IRAS 18151–1208. **(b)–(d)** Continuum-subtracted "narrow-band" images, in Brγ, H_2 1-0S(1), and [FeII] 1.644-μm emission, revealing line emission associated with accretion (Brγ) and a collimated jet (H_2 and [FeII]). The jet extends a few arcseconds to the southeast of the embedded source; the jet may in fact be driven by an unseen companion to the near-IR source, since it is offset slightly to the right. The features labeled B9 and B10 are H_2 emission knots in the extended counterflow.

be partially molecular, since not all H_2 features can be explained by the interaction of the jet with the ambient medium. The survival and collisional excitation of H_2 is only possible in oblique bow wings and, often, only if the preshock medium is already in motion. The H_2 must therefore have already passed through one or more bow shocks downwind. The H_2 must also survive these shocks, since at a density of ~10^4 cm^{-3} the timescale for H_2 reformation on grains is ~2×10^5 yr, comparable to the outflow dynamical timescale (*O'Connell et al.,* 2004). On the other hand, it has recently been proposed that gas phase H_2 formation in the warm, dust-free, partially ionized regions associated with internal working surfaces could account for the H_2 emission in some jets (*Raga et al.,* 2005).

Pulsed, precessing jet scenarios can be adopted to widen flows and produce the clusters of bows often seen in images of jets, like Cep A in Fig. 7 (e.g., *Völker et al.,* 1999; *Raga et al.,* 2004; *Smith and Rosen,* 2005a). It is interesting to note that, as is the case with many HH jets from TTS, some degree of variability is usually needed to produce the range of characteristics — chains of knots, multiple bows, broad cavities, etc. — observed in molecular flows.

[FeII] is often used to complement the molecular hydrogen data, as a probe of the higher-excitation, atomic jet component (*Reipurth et al.,* 2000; *Nisini et al.,* 2002a; *Giannini et al.,* 2002, 2004). [FeII] is particularly useful in regions where extinction inhibits optical studies, for example, in outflows from low-mass Class 0 sources or high-mass YSOs, or from the base of young jets close to the embedded protostar. With combined H- and K-band spectra, basic physical parameters can be traced along the jet axis. Where extinction is less extreme, e.g., where the jet breaks out of the circumstellar envelope, combined optical and near-IR studies can likewise be used to probe differing atomic gas components; the [FeII] 1.533/1.643 μm ratio, for example, probes densities up to 10^5 cm^{-3} (Fig. 9), one order of magnitude larger than those diagnosed through the [SII] 6716/6731 ratio (*Nisini et al.,* 2005). Because the [FeII] lines in the H band derive from levels with similar excitation energies (11,000–12,000 K), this ratio is almost independent of temperature. The [FeII] 1.643 μm/[SII] 1.03 μm or the [FeII] 1.25 μm/Paβ ratio can also potentially be used to estimate the fraction of iron in the gas phase, important when considering cooling, chemistry, and grain-sputtering processes in shocks, while the [FeII] 1.643 μm/[NI] 1.04 μm ratio can be used to estimate the ionization fraction and ultimately the jet mass flux (*Nisini et al.,* 2002a; *Giannini et al.,* 2004).

It is likely that most, if not all, of the infrared outflows that are detected in H_2 and [FeII] are embedded cases of HH flows that would have been seen in the optical if the extinction had been lower. An interesting transition case is

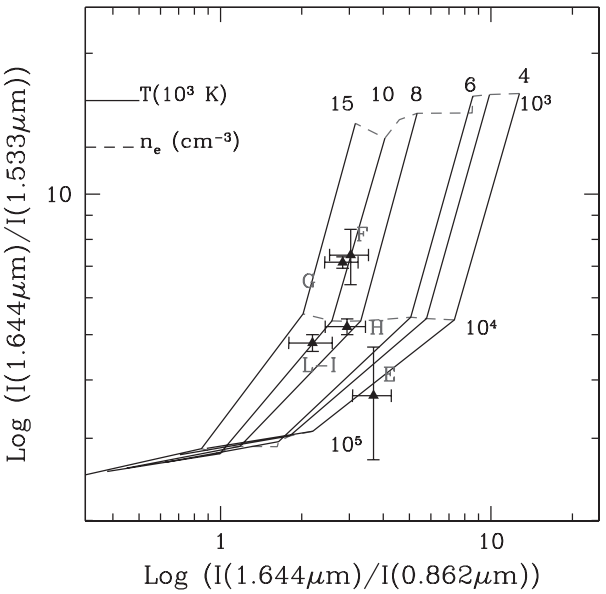

Fig. 9. Diagnostic diagram showing how [FeII] line ratios can be used to constrain the conditions in an ionized jet. The grid spans electron densities of 10^3, 10^4, and 10^5 cm^{-3} (dashed lines) and electron temperatures of 4, 5, 6, 8, 10, and 15×10^3 K (solid lines). Overplotted are line ratios extracted from near-IR spectra of the HH 1 jet. See *Nisini et al.* (2005) for details.

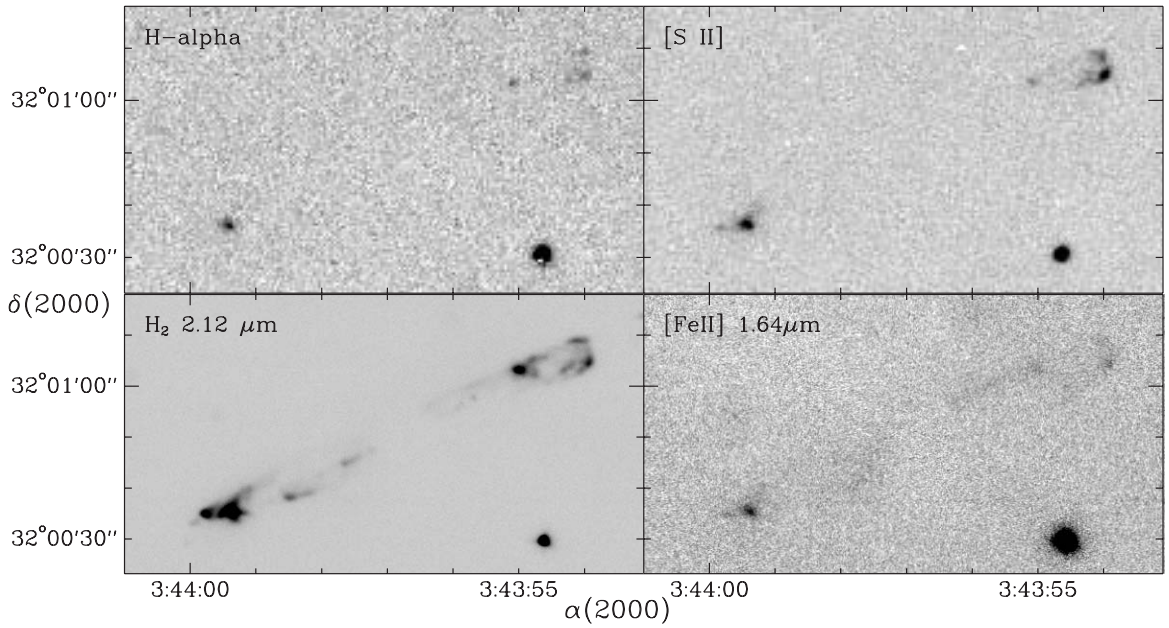

Fig. 10. The HH 211 flow emerges from a deeply embedded source in the IC 348 region in Perseus. The flow moves through a steep density gradient, and only the very outermost shock regions are visible as optical HH objects. From *Walawender et al.* (2006).

the HH 211 flow, which was originally discovered in the infrared (*McCaughrean et al.,* 1994). In the optical, only the outermost shock regions can be seen in Hα and [SII] (Fig. 10) (*Walawender et al.,* 2006).

4.2. Emission from the Jet Base: Constraining Jet Models

In the near-IR, considerable effort has also been spent on observing the central engine, particularly the region at the jet base within ~100 AU of the outflow source, where jets are collimated and accelerated. Prompted by the spectroscopic survey of *Reipurth and Aspin* (1997), and earlier optical studies of forbidden emission line (FEL) regions in TTS (e.g., *Hirth et al.,* 1997), *Davis et al.* (2001b, 2002, 2003) conducted a modest survey of Class I outflows at high spectral (although poor spatial) resolution (Fig. 11). Once again, H_2 and [FeII] proved to be important jet tracers, the H_2 delineating a slow (v_{rad} ~ 10–30 km s^{-1}), low-excitation, shocked molecular gas component (T ~ 2000K), with the [FeII] tracing a high-velocity (v_{rad} ~ 50–100 km s^{-1}), hot, dense, partially ionized region (T ~ 10,000K). While it seems likely that the [FeII] emission is closely tied to emission knots and shock fronts along the jet axis, the origin of the H_2 remains unclear; it could originate in the low-velocity wings of small bow shocks, from a turbulent boundary between the jet and ambient medium, or from a broad, cool component in a disk wind.

Spectro-astrometric techniques were employed to extract spatial information for the various kinematic components in each line. However, it was quickly realized that higher-spatial resolution was required, not least so that emission

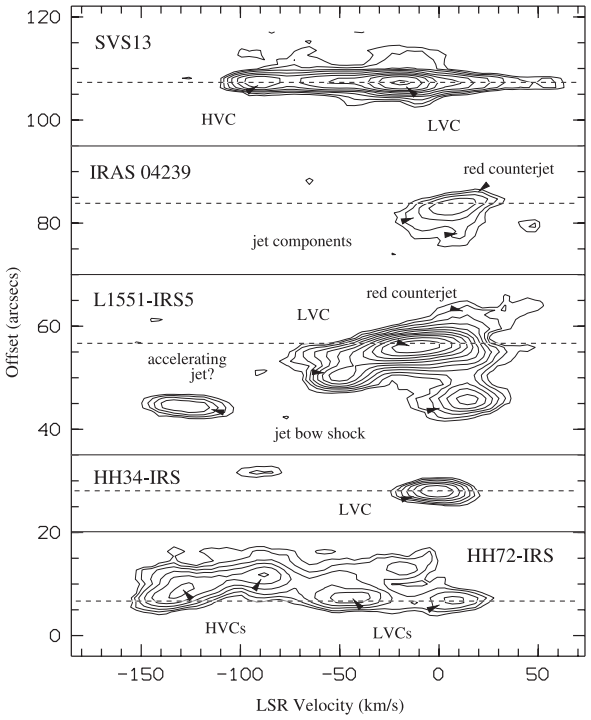

Fig. 11. Echelle spectral images showing the H_2 emission at the base of five molecular jets. The long slit was aligned with the jet axis in each region. The continuum (marked with a dashed line in each plot) has been fitted and removed from each dataset. Low-velocity H_2 is observed coincident with each outflow source, although spectro-astrometry usually indicates an offset, of the order of a few tens of AU, into the blue outflow lobe. Additional high-velocity shock features are seen along the jet axis in some flows. From *Davis et al.* (2001b).

at the "true jet base" could be distinguished from shock fronts further downwind. *Pyo et al.* (2002) and *Takami et al.* (2005) have since sought to characterize the kinematics and excitation of the atomic and molecular gas component on fine spatial scales, while *Davis et al.* (2006) have combined Subaru and Very Large Telescope (VLT) data to measure proper motions. Interestingly, in SVS 13 they measure a modest proper motion for the H_2 peak at the jet base, although they find that the [FeII] seems to be stationary. If confirmed with subsequent observations, this would suggest that the [FeII] is excited in a stationary shock, perhaps in a collimation point at the jet base.

The aim remains to constrain models of jet collimation and acceleration, distinguishing between X-wind and disk-wind models that to date have only been applied to relatively "evolved" YSOs (see the chapter by Ray et al.). Extending observational and theoretical studies to younger (Class 0/I) sources is important, particularly when one considers that a star's mass has largely been determined before the T Tauri phase, with accretion during the T Tauri phase adding only a small fraction to the final stellar mass.

Future observations, which *map* excitation and kinematics outward from the source, but also in the transverse direction across the width of the jet, will allow us to better test acceleration models, and also understand how energy and momentum are transferred from the jet to the ambient medium (e.g., *Chrysostomou et al.,* 2005). Near-IR integral field spectrometers, particularly those that offer high spectral resolution, or those with adaptive optics correction, should help further this cause.

4.3. Mid-Infrared Observations from Space

By extending infrared observations of jets to longer wavelengths, one has the opportunity to observe the very youngest flows, tracing emission from low-excitation regions (cool, molecular emission) but also from embedded, high-excitation jets (ionic emission) (reviewed by *van Dishoeck,* 2004). The Infrared Space Observatory (ISO) showed that essentially all the broadband mid-IR emission from outflows is due to lines. Again, H_2 and [FeII] are important coolants, via the pure rotational H_2 lines S(0)–S(7) between 5 and 30 μm, and the [FeII] forbidden emission lines, particularly those at 5.34, 17.94, 25.99, and 35.35 μm. The 17.03 μm H_2 v = 0–0 S(1) line, for example, from an energy level only 1015 K above the ground state, emits strongly from gas as cool as 100 K, while the [FeII] lines at 5.34 and 25.99 μm should be as strong as the 1.64 μm line, given conditions typical of protostellar jets (*Smith and Rosen,* 2005b; *Hartigan et al.,* 2004). Although the near- and mid-IR [FeII] lines trace similar flow components, the difference in extinction between 1 and 5 μm (on the order of 7) is potentially a problem and, with the launch of Spitzer, near-comparable spatial resolution is now possible.

As in the near-IR, H_2 and [FeII] line ratios can be used to test shock models and diagnose flow parameters. For example, the [FeII] 17.94 μm/5.34 μm and 25.99 μm/17.94 μm ratios can be used to constrain the density and temperature in the ionized flow (*White et al.,* 2000), while the H_2 S(5)/S(1) vs. S(5)/S(4) ratio diagram can be used to estimate shock velocities (*Molinari et al.,* 2000). The H_2 S(3) line at 9.67 μm can also be used to measure extinction, because it lies in the middle of a silicate absorption feature. A_v can thus be evaluated by aligning (or reducing the scatter) of H_2 column densities in a Boltzmann diagram, and particularly by adjusting A_v until the S(3) line converges toward the straight line defined by the other H_2 column densities.

Observations in transitions of other ionic species (e.g., [NeII] 12.81 μm, [NeIII] 15.55 μm, [SIII] 33.5 μm, [SiII] 34.82 μm) allow one to probe faster, higher-excitation shocks. For example, the [NeII] 12.81-μm line intensity is directly related to the shock velocity, requiring J shocks in excess of ~60 km s^{-1}, while [NeIII] 15.55-μm detections imply shock velocities exceeding 100 km s^{-1} (*Hollenbach and McKee,* 1989; *Molinari and Noriega-Crespo,* 2002; *Lefloch et al.,* 2003). With ISO these lines were only detected in massive YSO outflows, the exception being the high-excitation knots in HH 2. Nondetections in some high-excitation HH objects from low-mass YSOs were probably due to beam-filling effects, since the emitting regions, detected in optical high-excitation tracers like [OIII] 5007 emission, are known to be very small. Spitzer is proving to be more sensitive in this respect (e.g., *Noriega-Crespo et al.,* 2004a,b; *Morris et al.,* 2004).

Some ionic transitions, like [SiII] 34.82 μm, [FeII] 25.99 μm, and [FeII] 35.35 μm, can also be excited in intense UV fields, so although line ratios can be used to distinguish shock from PDR excitation, caution needs to be taken when analyzing data in some regions (e.g., *Froebrich et al.,* 2002).

At still longer wavelengths there are many important coolants for gas at temperatures between 300 and 1500 K (*Benedettini et al.,* 2000; *Molinari et al.,* 2000; *Giannini et al.,* 2001; *Smith et al.,* 2003b). Observations out to 200 μm have the potential to bridge the gap between the cold molecular flow components traced in the (sub)millimeter and the hot atomic/ionic shock tracers seen in the optical and near-IR. Indeed, the complete IR spectral coverage provided by ISO and Spitzer leads to a direct determination of the contribution of each species to the cooling, and a better overall estimate of the energy budget in each outflow. In Class 0 and Class I YSO flows, *Nisini et al.* (2002b) find that cooling from FIR lines is equivalent to a few percent of the source bolometric luminosity, the cooling from molecular lines being larger in outflows from Class 0 sources than in flows from Class I sources. Generally, CO, H_2, and H_2O contribute more or less equally to the cooling, although emission from gaseous water was conspicuously absent in many Class I YSO outflows, perhaps because of dissociation in shocks, dissociation by the interstellar FUV field, or freeze-out onto warm dust grains. Together these molecular lines radiate perhaps 50% of the mechanical power input by shocks, as one would expect from a momentum driven flow, where the mechanical power of the flow should be comparable to the energy radiated in the dissipative shocks. C-type shocks usually best fit the observed molecular line ratios — in outflows from low *and* high-mass YSOs — with

parameters similar to those inferred from near-IR observations (i.e. v_{sh} ~ 10–30 km s^{-1}; n_H ~ 10^4–10^6 cm^{-3}). However, a J-type component is also needed to explain the higher-excitation transitions (including [OI] 63-μm emission) seen in some regions, particularly in the Class I YSO flows. Note that the [CII] 158 μm/[OI] 63 μm fine-structure line ratio can be used to distinguish C from J shocks (being lower in the latter), provided the [CII] is not contaminated by emission from a PDR (*Benedettini et al.,* 2000; *Molinari and Noriega-Crespo,* 2002).

With ISO laying the groundwork, Spitzer is now in a position to build on these early results, by *spatially distinguishing* regions of hot (1000–3000 K) molecular material from cool (200–1000 K) molecular gas in extended bow shocks and thereby fine-tuning combined C- plus J-type (or J-type plus magnetic precursor) shock models. Detecting jets from the most embedded flows, from very low-mass YSOs, and from distant, high-mass YSOs should also be possible.

Acknowledgments. C.J.D. would like to thank M. Smith, B. Nisini, D. Froebrich, and A. Noriega-Crespo for their comments and suggestions. J.B. thanks P. Hartigan for suggestions regarding the interpretation of the HH 444 jet spectra. We thank the referee, A. Raga, for helpful comments. This work was supported by the NASA Astrobiology Institute under Cooperative Agreement No. NNA04CC08A issued through the Office of Space Science.

REFERENCES

Andrews S. M., Reipurth B., Bally J., and Heathcote S. R. (2004) *Astrophys. J., 606,* 353–368.

Bachiller R., Guilloteau S., Gueth F., Tafalla M., Dutrey A., Codella C., and Castets A. (1998) *Astron. Astrophys., 339,* L49–L52.

Bachiller R., Gueth F., Guilloteau S., Tafalla M., and Dutrey A. (2000) *Astron. Astrophys., 362,* L33–L36.

Bally J. and Devine D. (1994) *Astrophys. J., 428,* L65–L68.

Bally J. and Reipurth B. (2001) *Astrophys. J., 546,* 299–323.

Bally J., Devine D., and Reipurth B. (1996) *Astrophys. J., 473,* L49–L52.

Bally J., O'Dell C. R., and McCaughrean M. J. (2000) *Astron. J., 119,* 2919–2959.

Bally J., Johnstone D., Joncas G., Reipurth B., and Mallén-Ornelas G. (2001) *Astron. J., 122,* 1508–1524.

Bally J., Heathcote S., Reipurth B., Morse J., Hartigan P., and Schwartz R. D. (2002a) *Astron. J., 123,* 2627–2657.

Bally J., Reipurth B., Walawender J., and Armond T. (2002b) *Astron. J., 124,* 2152–2163.

Bally J., Reipurth B., and Aspin C. (2002c) *Astrophys. J., 574,* L79–L82.

Bally J., Feigelson E., and Reipurth B. (2003) *Astrophys. J., 584,* 843–852.

Bally J., Licht D., Smith N., and Walawender J. (2005) *Astron. J., 129,* 355–362.

Bally J., Licht D., Smith N., and Walawender J. (2006) *Astron. J., 131,* 473–500.

Benedettini M., Giannini T., Nisini B., et al. (2000) *Astron. Astrophys., 359,* 148–158.

Cernicharo J., Lefloch B., Cox P., Cesarsky D., Esteban C., et al. (1998) *Science, 282,* 462–465.

Chrysostomou A., Bacciotti F., Nisini B., Ray T. P., Eislöffel J., Davis C. J., and Takami M. (2005) *PPV Poster Proceedings.* Available on line at http://www.lpi.usra.edu/meetings/ppv2005/pdf/8156.pdf.

Davis C. J., Hodapp K. W., and Desroches L. (2001a) *Astron. Astrophys., 377,* 285–296.

Davis C. J., Ray T. P., Desroches L., and Aspin C. (2001b) *Mon. Not. R. Astron. Soc., 326,* 524–538.

Davis C. J., Stern L., Ray T. P., and Chrysostomou A. (2002) *Astron. Astrophys., 382,* 1021–1031.

Davis C. J., Whelan E., Ray T. P., and Chrysostomou A. (2003) *Astron. Astrophys., 397,* 693–710.

Davis C. J., Varricatt W. P., Todd S. P., and Ramsay Howat S. K. (2004) *Astron. Astrophys., 425,* 981–995.

Davis C. J., Nisini B., Takami M., Pyo T. S., Smith M. D., et al. (2006) *Astrophys. J., 639,* 969–974.

Devine D., Bally J., Reipurth B., and Heathcote S. (1997) *Astron. J., 114,* 2095–2111.

Devine D., Reipurth B., and Bally J. (1999) *Astron. J., 118,* 972–982.

Devine D., Bally J., Reipurth B., Stocke J., and Morse J. (2000a) *Astrophys. J., 540,* L57–L59.

Devine D., Grady C. A., Kimble R. A., Woodgate B., Bruhweiler F. C., Boggess A., Linsky J. L., and Clampin M. (2000b) *Astrophys. J., 542,* L115–L118.

Dopita M. A., Schwartz R. D., and Evans I. (1982) *Astrophys. J., 263,* L73–L77.

Downes T. and Cabrit S. (2003) *Astron. Astrophys., 403,* 135–140.

Eislöffel J. (2000) *Astron. Astrophys., 354,* 236–246.

Eislöffel J. and Mundt R. (1997) *Astron. J., 114,* 280–287.

Eislöffel J., Froebrich D., Stanke T., and McCaughrean M. J. (2003) *Astrophys. J., 595,* 259–265.

Favata F., Fridlund C. V. M., Micela G., Sciortino S., and Kaas A. A. (2002) *Astron. Astrophys., 386,* 204–210.

Flower D. R., Le Bourlot J., Pineau des Forêts G., and Cabrit S. (2003) *Mon. Not. R. Astron. Soc., 341,* 70–80.

Froebrich D., Smith M. D., and Eislöffel J. (2002). *Astron. Astrophys., 385,* 239–256.

Giannini T., Nisini B., and Lorenzetti D. (2001) *Astrophys. J., 555,* 40–57.

Giannini T., Nisini B., Caratti o Garatti A., and Lorenzetti D. (2002) *Astrophys. J., 570,* L33–L36.

Giannini T., McCoey C., Caratti o Garatti A., Nisini B., Lorenzetti D., and Flower D. R. (2004) *Astron. Astrophys., 419,* 999–1014.

Grady C. A., Woodgate B., Torres C. A. O., Henning Th., Apai D., et al. (2004) *Astrophys. J., 608,* 809–830.

Grady C. A., Woodgate B. E., Bowers C. W., Gull T. R., Sitko M. L., et al. (2005) *Astrophys. J., 630,* 958–875.

Gull T. R. and Sofia S. (1979) *Astrophys. J., 230,* 782–785.

Haro G. (1952) *Astrophys. J., 115,* 572–572.

Haro G. (1953) *Astrophys. J., 117,* 73–82.

Hartigan P.,Morse J. A., Tumlinson J., Raymond J., and Heathcote S. (1999) *Astrophys. J., 512,* 901–915.

Hartigan P., Raymond J., and Pierson R. (2004) *Astrophys. J., 614,* L69–L71.

Hatchell J., Richer J. S., Fuller G. A., Qualtrough C. J., Ladd E. F., and Chandler C. J. (2005) *Astron. Astrophys., 440,* 151–161.

Herbig G. H. (1950) *Astrophys. J., 111,* 11–14.

Herbig G. H. (1951) *Astrophys. J., 113,* 697–699.

Herbig G. H. and Jones B. F. (1981) *Astron. J., 86,* 1232–1244.

Hirth G., Mundt R., and Solf J. (1997) *Astron. Astrophys. Suppl., 126,* 437–469.

Hollenbach D. and McKee C. F. (1989) *Astrophys. J., 342,* 306–336.

Kastner J. H., Franz G., Grosso N., Bally J., McCaughrean M. J., Getman K., Feigelson E. D., and Schulz N. S. (2005) *Astrophys. J. Suppl., 160,* 511–529.

Khanzadyan T., Gredel R., Smith M. D., and Stanke T. (2004a) *Astron. Astrophys., 426,* 171–183.

Khanzadyan T., Smith M. D., Davis C. J., and Stanke T. (2004b) *Astron. Astrophys., 418,* 163–176.

Knee L. B. G. and Sandell G. (2000) *Astron. Astrophys., 361,* 671–684.

Le Bourlot J., Pineau des Forêts G., Flower D. R., and Cabrit S. (2002) *Mon. Not. R. Astron. Soc., 332,* 985–993.

Lee C. F., Stone J. M., Ostriker E. C., and Mundy L. G. (2001) *Astrophys. J., 557,* 429–442.

Lefloch B., Cernicharo J., Cabrit S., Noriega-Crespo A., Moro-Martín A., and Cesarsky D. (2003) *Astrophys. J., 590,* L41–L44.

Lizano S., Heiles C., Rodríguez L. F., Koo B. C., Shu F. H., et al. (1988) *Astrophys. J., 328,* 763–776.
Masciadri E. and Raga A. C. (2001) *Astron. J., 121,* 408–412.
McCaughrean M. J., Rayner J. T., and Zinnecker H. (1994) *Astrophys. J., 436,* L189–L192.
McCoey C., Giannini T., Flower D. R., and Caratti o Garatti A. (2004) *Mon. Not. R. Astron. Soc., 353,* 813–824.
Miesch M. S. and Bally J. (1994) *Astrophys. J., 429,* 645–671.
Miesch M. S., Scalo J., and Bally J. (1999) *Astrophys. J., 524,* 895–922.
Molinari S. and Noriega-Crespo A. (2002) *Astron. J., 123,* 2010–2018.
Molinari S., Noriega-Crespo A., Ceccarelli C., Nisini B., Giannini T., et al. (2000) *Astrophys. J., 538,* 698–709.
Morris P. W., Noriega-Crespo A., Marleau F. R., Teplitz H. I., Uchida K. I., and Armus L. (2004) *Astrophys. J. Suppl., 154,* 339–345.
Mundt R. and Fried J. W. (1983) *Astrophys. J., 274,* L83–L86.
Nisini B., Caratti o Garatti A., Giannini T., and Lorenzetti D. (2002a) *Astron. Astrophys., 393,* 1035–1051.
Nisini B., Giannini T., and Lorenzetti D. (2002b) *Astrophys. J., 574,* 246–257.
Nisini B., Bacciotti F., Giannini T., Massi F., Eislöffel J., et al. (2005) *Astron. Astrophys., 441,* 159–170.
Noriega-Crespo A., Moro-Martin A., Carey S., Morris P. W., Padgett D. L., et al. (2004a) *Astrophys. J. Suppl., 154,* 402–407.
Noriega-Crespo A., Morris P., Marleau F. R., Carey S., Boogert A., et al. (2004b) *Astrophys. J. Suppl., 154,* 352–358.
O'Connell B., Smith M. D., Davis C. J., Hodapp K. W., Khanzadyan T., and Ray T. P. (2004) *Astron. Astrophys., 419,* 975–990.
O'Connell B., Smith M. D., Froebrich D., Davis C. J., and Eislöffel J. (2005) *Astron. Astrophys., 431,* 223–234.
Ogura K. (1991) *Astron. J., 101,* 1803–1806.
Ogura K. (1995) *Astrophys. J., 450,* L23–L26.
Phelps R. L. and Barsony M. (2004) *Astron. J., 127,* 420–443.
Pound M. W. and Bally J. (1991) *Astrophys. J., 383,* 705–713.
Pravdo S. H. and Tsuboi Y. (2005) *Astrophys. J., 626*, 272–282.
Pravdo S. H., Feigelson E. D., Garmire G., Maeda Y., Tsuboi Y., and Bally J. (2001) *Nature, 413,* 708–711.
Pravdo S. H., Tsuboi Y., and Maeda Y. (2004) *Astrophys. J., 605,* 259–271.
Pyo T-S., Hayashi M., Kobayashi N., Terada H., Goto M., et al. (2002) *Astrophys. J., 570,* 724–733.
Raga A. C., Noriega-Crespo A., and Velázquez P. F. (2002) *Astrophys. J., 576,* L149–L152.
Raga A. C., Noriega-Crespo A., González R. F., and Veázquez P. F. (2004) *Astrophys. J. Suppl., 154,* 346–351.
Raga A. C., Williams D. A., and Lim A. J. (2005) *Rev. Mex. Astron. Astrofis., 41,* 137–146.
Reipurth B. (2000) *Astron. J., 120,* 3177–3191.
Reipurth B. and Aspin C. A. (1997) *Astron. J., 114,* 2700–2707.
Reipurth B. and Aspin C. A. (2004) *Astrophys. J., 608,* L65–L68.
Reipurth B. and Bally J. (2001) *Ann. Rev. Astron. Astrophys., 39,* 403–455.
Reipurth B., Bally J., Graham J. A., Lane A. P., and Zealey W. J. (1986) *Astron. Astrophys., 164,* 51–66.
Reipurth B., Bally J., and Devine D. (1997) *Astron. J., 114,* 2708–2735.
Reipurth B., Bally J., Fesen R. A., and Devine D. (1998a) *Nature, 396,* 343–345.
Reipurth B., Devine D., and Bally J. (1998b) *Astron. J., 116,* 1396–1411.
Reipurth B., Yu K. C., Heathcote S., Bally J., and Rodríguez L. F. (2000) *Astron. J., 120,* 1449–1466.
Reipurth B., Armond T., Raga A., and Bally J. (2003) *Astrophys. J., 593,* L47–L50.
Reipurth B., Yu K. C., Moriarty-Schieven G., Bally J., Aspin C., and Heathcote S. (2004) *Astron. J., 127,* 1069–1080.
Rodríguez L. F., Escalante V., Lizano S., Cantó J., and Mirabel I. F. (1990) *Astrophys. J., 365,* 261–268.
Rodríguez L. F., Anglada G., and Curiel S. (1997) *Astrophys. J., 480,* L125–L128.
Rodríguez L. F., Anglada G., and Curiel S. (1999) *Astrophys. J. Suppl., 125,* 427–438.
Rosen A. and Smith M. D. (2004) *Mon. Not. R. Astron. Soc., 347,* 1097–1112.
Rudolph A. L., Bachiller R., Rieu, N. Q., Van Trung D., Palmer P., and Welch W. J. (2001) *Astrophys. J., 558,* 204–215.
Schultz A. S. B., Burton M. G., and Brand P. W. J. L. (2005) *Mon. Not. R. Astron. Soc., 358,* 1195–1214.
Smith M. D. and Rosen A. (2005a) *Mon. Not. R. Astron. Soc., 357,* 579–589.
Smith M. D. and Rosen A. (2005b) *Mon. Not. R. Astron. Soc., 357,* 1370–1376.
Smith M. D., Khanzadyan T., and Davis C. J. (2003a) *Mon. Not. R. Astron. Soc., 339,* 524–536.
Smith M. D., Froebrich D., and Eislöffel J. (2003b) *Astrophys. J., 592,* 245–254.
Smith N., Bally J., and Brooks K. J. (2004) *Astron. J., 127,* 2793–2808.
Smith N., Bally J., Licht D., and Walawender J. (2005) *Astron. J., 129,* 382–392.
Snell R. L., Loren R. B., and Plambeck R. L. (1980) *Astrophys. J., 239,* L17–L22.
Stanke T. (2000) Ph.D. thesis, Univ. of Potsdam.
Stanke T., McCaughrean M. J., and Zinnecker H. (1998) *Astron. Astrophys., 332,* 307–313.
Stanke T., McCaughrean M. J., and Zinnecker H. (1999) *Astron. Astrophys., 350,* L43–L46.
Stanke T., McCaughrean M. J., and Zinnecker H. (2000) *Astron. Astrophys., 355,* 639–650.
Stanke T., McCaughrean M. J., and Zinnecker H. (2002) *Astron. Astrophys., 392,* 239–266.
Strom S. E., Vrba F. J., and Strom K. M. (1976) *Astron. J., 81,* 314–316.
Takami M., Chrysostomou A., Ray T. P., Davis C. J., Dent W. R. F., et al. (2005) *PPV Poster Proceedings.* Available on line at http://www.lpi.usra.edu/meetings/ppv2005/pdf/8207.pdf.
van Dishoeck E. F. (2004) *Ann. Rev. Astron. Astrophys., 42,* 119–167.
Völker R., Smith M. D., Suttner G., and Yorke H. W. (1999) *Astron. Astrophys., 343,* 953–965.
Wang M., Noumaru J., Wang H., Yang J., and Chen J. (2005) *Astron. J., 130,* 2745–2756.
Walawender J., Bally J., Reipurth B., and Aspin C. (2004) *Astron. J., 127,* 2809–2816.
Walawender J., Bally J., and Reipurth B. (2005) *Astron. J., 129,* 2308–2351.
Walawender J., Bally J., Kirk H., Johnstone D., Reipurth B., and Aspin C. (2006) *Astron J., 132,* 467–477.
White G. W., Liseau R., Men'shchikov A. B., Justtanont K., Nisini B., et al. (2000) *Astron. Astrophys., 364,* 741–762.
Wilking B. A., Schwartz R. D., Fanetti T. M., and Friel E. D. (1997) *Publ. Astron. Soc. Pac., 109,* 549–553.
Wu Y., Wei Y., Zhao M., Shi Y., Yu W., Qin S., and Huang M. (2004) *Astron. Astrophys., 426,* 503–515.